Author Manuscript

Evaluating pressure-dependent discharge behavior of foil versus *in situ* plated lithium metal anodes in solid-state batteries

Catherine G. Haslam[1,6], Janis K. Eckhardt[2], Abhinand Ayyaswamy[3,6], Bairav S. Vishnugopi[3,6], Till Fuchs[2], Daniel W. Liao[4], Neil P. Dasgupta[1,4,6], Partha P. Mukherjee[3,6], Jürgen Janek[2], and Jeff Sakamoto[5,6]*

[1] Department of Materials Science and Engineering, University of Michigan, Ann Arbor, MI 48109, United States

[2] Institute of Physical Chemistry and Center for Materials Research (ZfM), Justus Liebig University, Giessen 35392, Germany

[3] School of Mechanical Engineering, Purdue University, West Lafayette, IN 47907, United States

[4]Department of Mechanical Engineering, University of Michigan, Ann Arbor, MI 48109, United States

[5]Materials Department, University of California Santa Barbara, Santa Barbara, CA 93106, United States

[6] MUSIC DOE Energy Frontier Research Center, University of Michigan, Ann Arbor, MI 48109, United States

*Corresponding author: sakamoto@ucsb.edu

Abstract

Anode-free manufacturing of solid-state batteries (SSBs) shows promise to maximize energy density by eliminating excess lithium (Li) and simplifying battery production. However, high reversibility during discharge (stripping of Li) is necessary for long-lifetime SSBs with a limited Li reservoir. Further, the plastic flow of Li changes depending on the Li thickness, leading to possible differences in discharge performance under stack pressure. This work investigates the pressure-dependent discharge performance of anode-free manufactured SSBs with *in situ* plated Li and compares the performance to that of conventional thick Li foil cells. Distinct stripping behavior is observed at low pressures (0-1 MPa), where Li diffusivity and initial interfacial contact may control accessible capacity, compared to high pressures (3-10 MPa) where mechanical deformation of Li likely governs stripping behavior.

This is the author manuscript accepted for publication and has undergone full peer review but has not been through the copyediting, typesetting, pagination and proofreading process, which may lead to differences between this version and the Version of Record. Please cite this article as doi: 10.1002/aenm.202403614.

This article is protected by copyright. All rights reserved.

Author Manuscript

Analysis of impedance spectra collected during stripping shows that additional stack pressure delays the formation of deep, as opposed to lateral, voids in the Li anode. These results provide insights to guide the transition from thick Li foil anodes to anode-free manufactured SSBs.

Introduction

There is potential for solid-state batteries (SSBs) to play a key role in vehicle electrification due to increased safety and higher energy density than current Li-ion batteries [1–4]. The increased energy density expected from SSBs comes from enabling the Li metal anode (q_{th} = 3860 mAh g^{-1}) to replace the graphite anode (q_{th} = 372 mAh g^{-1}) in conventional Li-ion batteries [5,6]. Commercial cells will require Li metal anodes with a thickness ≤ 25 μm to realize its energy density benefits [7]. However, many studies utilize Li foil with a thickness of 100-750 μm to examine the electrochemical behavior of Li anodes in SSBs [8–12]. The air sensitivity of Li metal makes processing Li foils to ≤100 μm thickness difficult, while integrating Li foil with the solid-state electrolyte (SSE) to form a clean interface provides additional challenges [13–16].

"Anode-free" (or "Li-metal-free") manufacturing of SSBs is an attractive solution to avoid the processing steps associated with handling Li metal [17–23]. In these cells, the anode-side current collector (CC) is bare when the cell is formed. All of the Li is stored in the pre-lithiated cathode, such as $LiNi_xMn_yCo_zO_2$, and plated on the anode CC during the first charging cycle. Here, the Li anode is referred to as *in situ* plated to distinguish from pre-existing Li foil integrated during cell manufacturing. This design eliminates excess Li in the cell, giving the highest energy density possible, and could simultaneously decrease costs by eliminating manufacturing steps associated with Li foil processing [24].

One factor limiting the use of Li metal anodes in SSBs is the challenge of maintaining contact at the solid|solid interface between Li metal and the SSE during discharge (stripping) [8,10,25–27]. The flux of vacancies into the Li metal anode, determined by the stripping current density, must be balanced by diffusion of Li/vacancies or creep of Li induced by stack pressure to maintain interfacial Li|SSE contact.

This article is protected by copyright. All rights reserved.

If these conditions are not met, the vacancies at the Li|SSE interface may coalesce into voids, which then reduce the Li|SSE contact area. The decreased contact between the Li metal anode and SSE increases the cell resistance, leading to cell polarization and restricts further stripping of Li [28,29]. This limits the capacity of Li that can be accessed, decreasing the effective energy density of the cell. Furthermore, the formation of voids in Li can be a precursor to cell failure during the subsequent charge cycle [27,30–34]. Therefore, preventing void formation in the Li metal anode during stripping is crucial to both prevent cell failure and maximize the accessible capacity of the cell.

Void formation during Li stripping is mitigated in many studies by applying high stack pressures (> 5 MPa) to facilitate creep of Li metal, and/or by increasing the cell temperature (> 25°C) to enhance Li diffusivity and mechanical deformation [16,25,27,35–37]. These strategies are useful on the laboratory scale to study the Li|SSE interface, but in commercial SSBs the stack pressure is limited to ≤ 1 MPa without further engineering controls that would decrease the overall pack level energy density [7,24]. Previous work has assessed the effect of pressure on Li stripping performance using thick Li foils (100-750 µm) and stripping a small fraction of the overall Li capacity (6-15%) at low current densities (0.2-0.4 mA cm^{-2}) [8,10]. Higher operational current densities ~1 mA cm^{-2} are needed to compete with LIBs, and SSB performance must be evaluated in this range [3,38,39]. While these studies have formed a strong foundation for Li stripping in SSBs, the thick Li foils used and large amount of excess Li present in these experiments may impact the overall cell performance compared to “anode-free” SSBs with no excess Li.

In this work, we investigate the pressure-dependent discharge performance of Li metal anodes in garnet-type $Li_{6.5}La_3Ta_{0.5}Zr_{1.5}O_{12}$ (LLZO) SSBs in both “anode-free” cells with *in situ* plated Li metal and symmetric cells with conventional thick Li foils. Additionally, the impact of temperature on the stripping behavior of *in situ* plated Li at constant pressure is assessed. Here, we use a commercially relevant stripping current density of 1 mA cm^{-2}. Different stripping behavior is observed in the low-pressure regime (0-1 MPa) where Li diffusion or the initial Li|LLZO contact are believed to be the dominant factors in discharge behavior, compared to the typical testing range of SSBs (3-10 MPa) where creep of Li is believed to control Li stripping performance. For both Li foil and *in situ* plated Li

This article is protected by copyright. All rights reserved.

Author Manuscript

anodes, similar trends in increased discharge capacity are observed with increase in pressure. These results highlight the importance of the Li anode processing and SSE interfacial formation steps on the stripping performance of SSBs.

Experimental

Materials

LLZO billets (d = 12.7 mm) with the composition $Li_{6.5}La_3Ta_{0.5}Zr_{1.5}O_{12}$ were densified using rapid-induction hot-pressing, as described previously [12]. Each billet was cut into pellets ranging in thickness from 2-3 mm using a diamond saw. X-ray diffraction (Rigaku Corp.) was used to confirm the phase purity of the LLZO pellets after hot-pressing. The pellets were ground with sandpaper (220, 400, 1200 grit) followed by a sequence of polishing steps using diamond paste up to a final particle size of 0.1 μm. For the *in situ* formed Li cells, a battery grade Cu foil (Targray) with thickness 10 μm was laminated to the LLZO surface at 900°C under 3.15 MPa pressure for 5 minutes [21]. Next, the opposite face of the LLZO pellet was polished to a final particle size of 0.1 μm. The polished pellets were heat treated to 400°C in an argon-filled glovebox (Vacuum Atmospheres Co.) with oxygen content < 1 ppm, which has been shown previously to remove contaminants from the LLZO surface [15]. The Li foil was prepared by rolling a Li rod (Albemarle, 99.9% purity) in a dry room (-50°C dew point) down to a final thickness of 300 μm. This thick Li foil was used as the counter electrode for *in situ* formed Li cells, and as both the counter and working electrode in Li foil cells. The Li/LLZO interface was prepared by scraping the oxide layer on Li foil before punching the Li into discs and applying it to the LLZO surface. Discs of 35 μm thick battery-grade Ni foil (Targray) were pressed on the back surface of the Li foil. Then, the cells were compressed under 5 MPa stack pressure for ~60 seconds to adhere the Li to the LLZO surface. Finally, the cells were conditioned at 170°C for 15-20 hours at ~1 MPa inside the glovebox to enhance Li/LLZO contact. Both cell types utilized larger surface area counter electrodes (diameter = 12.7 mm) relative to the working electrode area (diameter = 6 mm) to minimize the risk of short-circuiting during Li plating on the counter electrode.

Electrochemical Testing

This article is protected by copyright. All rights reserved.

Author Manuscript

Author Manuscript

All electrochemical testing was performed using a Bio-logic VMP-300 potentiostat. Stack pressure was applied to cells during electrochemical testing using a load frame (IMADA) with custom pressure clamp. The *in situ* plated Li anode was formed at 60°C by plating Li from the thick Li foil counter electrode to the bare Cu CC using a pulsed current protocol to enhance plated Li homogeneity as described by Lee *et al* [40]. The stack pressure during *in situ* Li plating was 5 MPa, and the Cu CC was backed by a polished stainless-steel disc to improve Li homogeneity. A high initial pulsed current density of 1 mA cm^{-2} was applied for the first 0.2 mAh cm^{-2}, followed by constant current plating at 0.2 mA cm^{-2} for the remaining 3.1 mAh cm^{-2}. Due to the elevated temperature (60°C) and stack pressure (5 MPa), no polarization during stripping of the Li foil counter electrode was observed during *in situ* Li plating. Therefore, we assume that changes to the Li foil counter electrode are negligible and do not affect subsequent stripping of the *in situ* plated Li. All Li stripping experiments in the pressure series were performed at room temperature (25 °C) and current density of 1 mA cm^{-2} under varying stack pressure. For examination of the temperature dependence of stripping performance, experiments were performed at a constant pressure of 3 MPa and current density of 1 mA cm^{-2} while the cell temperature was varied to 25, 50, or 75 °C. Galvanostatic electrochemical impedance spectroscopy (GEIS) was conducted during stripping to assess changes in the Li|LLZO interface. An AC perturbation current of 0.05 mA cm^{-2} oscillating around the DC stripping current was applied over a frequency range of 7 MHz to 1 Hz. Potentiostatic electrochemical impedance spectroscopy (PEIS) was also performed on the cells as-assembled (before *in situ* plating), after *in situ* plating, and after the cells polarized during stripping to assess interface recovery. An AC perturbation voltage of 5 mV was applied over a frequency range of 7 MHz to 1 Hz.

Materials Characterization

Optical microscopy of the Cu CC beneath which the *in situ* Li was plated was performed with a VHX-7000 4k digital microscope (Keyence) inside an argon glovebox. The *in situ* plated Li cross section was cut using plasma focused ion beam milling with a Helios G4 Dual Beam FIB/SEM (ThermoFisher). Cross sections were cut using a beam current of 0.50 µA and accelerating voltage of 30 kV. Scanning

This article is protected by copyright. All rights reserved.

electron microscopy images were acquired on the same system using a beam current of 0.2 nA and accelerating voltage of 3 kV.

Electron Backscatter Diffraction

To prepare the *in situ* plated Li cross section for analysis, the *in situ* plated Li cell was fractured perpendicular to the sample surface as described by Fuchs *et al* [41]. The fractured cross section was then further processed using plasma FIB (XEIA3 system, Tescan). FIB milling was conducted at -130°C and a beam current 0.1-2.7 µA and beam voltage 30 kV. Li foil was prepared for analysis by first conducting the same sample preparation steps as Li foil undergoes in the symmetric cells used in the stripping experiments. First, the Li foil surface was lightly scraped in the glovebox to remove the oxide layer. Next, the Li foil was pressed at 5 MPa for ~60 seconds between two stainless steel foils (20 µm thick), as the stainless steel improves the quality of the milling. Finally, the Li foil was conditioned at 170°C for 15-20 hours at ~1 MPa inside the glovebox to match the procedure carried out for assembly of Li foil|LLZO cells. This stack was cut then by scissors and the resulting cross-section polished similarly to the fractured cross-section described earlier with FIB at -130°C. The samples were transferred to the SEM (Gemini 560, Carl Zeiss Microscopy) under inert and cryogenic conditions using a VCT500 transfer module (Leica Microsystems). Microstructural characterization was performed using a Symmetry 3 EBSD detector (Oxford Instruments), and analysis was carried out at 20 kV. Post-processing of the recorded EBSD maps was performed using the AZtecCrystal software (Oxford Instruments).

Analysis of Experimental Impedance Spectra

The collected impedance data were analyzed in the time domain using the commercial software RelaxIS 3 (version 3.0.22.29, rhd instruments GmbH & Co. KG.). Records in the high- and low-frequency range with residuals greater than 3% in the Kramers-Kronig test were not included in data evaluation [42]. Only the real part of the impedance is considered during analysis, since the residuals are in the range of a few 0.1% only. No additional data points were generated by interpolation, and the second derivative of the

This article is protected by copyright. All rights reserved.

Author Manuscript

distribution function $\gamma(\tau)$ with a lambda parameter of 10^{-3} was used in the Tikhonov regularization problem [43].

Coupled electrochemical-mechanical modeling framework

A mechanistic modeling framework is developed to compute the Li|SSE interface evolution and the contact overpotential during stripping at various operating conditions. The evolving interface captured from the model stems from the relative competition of multi-mechanistic processes at various phases of operation. The void depth at the Li|SSE interface is governed by the following competing mechanisms: (a) contact mechanics (b) Li creep, (c) Li self-diffusion, and (d) electrochemical reaction. A detailed description of the model developed can be found in the Supporting Information, including the roughness profile generation, contact mechanics, Li creep, Li self-diffusion, electrochemical reaction, and temperature dependence of properties.

Results and Discussion

Currently, the detailed effects of pressure and temperature on the discharge performance of *in situ* plated Li compared to conventional Li foils in SSBs are unknown. Therefore, two types of Li anodes were formed on the LLZO surface to investigate the effect of pressure and temperature during Li stripping. The stripping experiments were performed 5 times for each of the chosen pressure or temperature condition to account for variations between samples and attain a standard deviation at each condition (Table S3).

First, Li was plated *in situ* at 60°C following the method of Lee *et al.* to form a homogenous layer of Li (Figure 1a) [40]. The uniformity of the *in situ* plated Li was measured using optical microscopy and cross-sectional scanning electron microscopy imaging, which confirmed that the thickness of the Li matched the expected capacity plated (Figure S1). PEIS was performed before and after *in situ* plating to confirm that there was no short circuiting of the cell during Li plating (Figure S2). Li foil cells were fabricated following the method of Sharafi *et al.* to achieve a low Li|LLZO interfacial resistance (Figure 1b) [15]. While these cell types represent current laboratory protocol standards for formation of "anode-

This article is protected by copyright. All rights reserved.

Author Manuscript

Author Manuscript

free" and Li foil cells, respectively, the effects of variations in processing temperature and Li integration between these cell types on discharge performance has not been comparatively studied in detail.

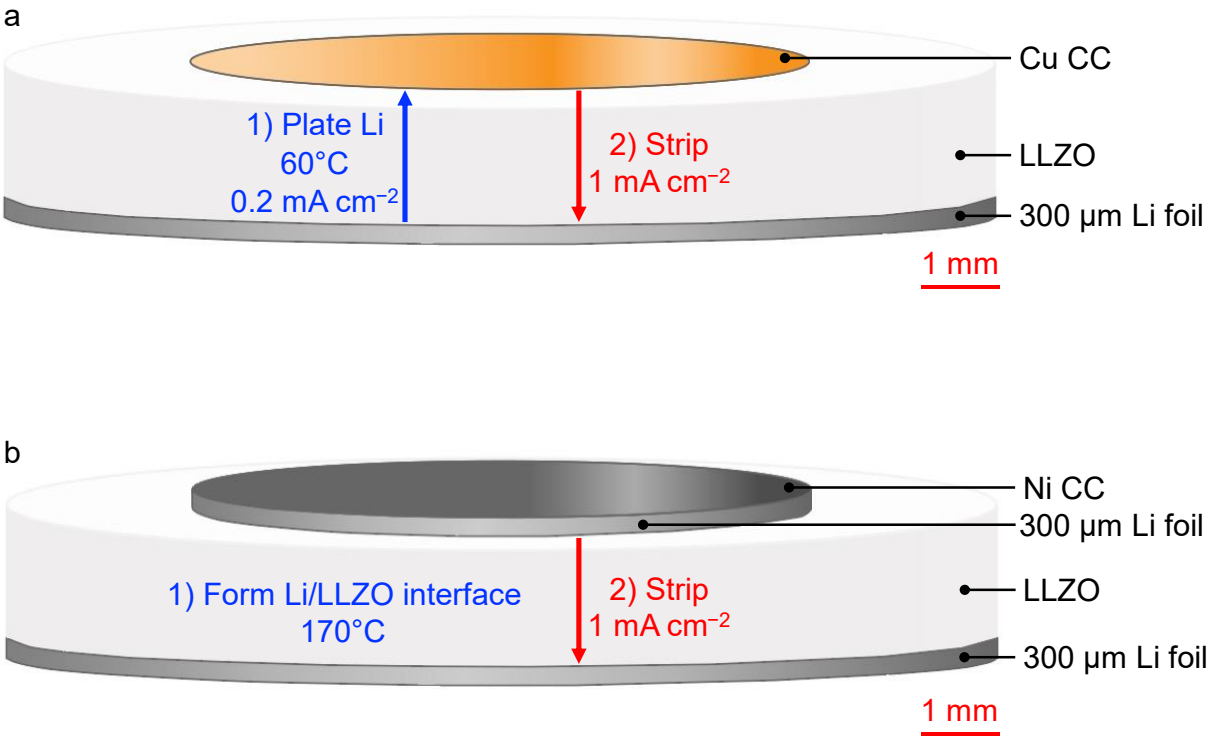


Figure 1. Schematic of **a** in situ and **b** Li foil cells using for stripping experiments.

Following the formation of the two types of Li anodes, the cells were cooled to room temperature. A range of stack pressures were applied to the cells during stripping (0, 1, 3, 5, and 10 MPa). For *in situ* plated Li, the cell temperature was also varied (25, 50, 75°C) during stripping at constant pressure of 3 MPa. The 0 – 1 MPa stack pressure range was investigated because it is of commercial relevance, as additional engineering controls would be required to achieve stack pressures >1 MPa in commercial SSBs [7,24]. Here, the 3-10 MPa stack pressure range is studied as a comparison to common stack pressures used in SSB research. 10 MPa was chosen as a maximum because stack pressures of 10 MPa and above have been shown to accelerate short-circuiting of sulfide-based SSBs [44].

This article is protected by copyright. All rights reserved.

Author Manuscript

For all cells, unidirectional stripping of Li was carried out at a constant current of 1 mA cm^{-2}. Unidirectional stripping of Li follows the suggestion of Fuchs *et al*. to probe the properties of the lithium metal anode itself, without convolution from the SSE or cycling [45]. *Operando* GEIS analysis was used to gain further insight into the evolution of dynamic kinetic interfacial phenomena while stripping at 1 mA cm^{-2}. Utilizing GEIS allows for the deconvolution of different contributions to cell impedance during stripping that lead to voltage polarization. Of significant interest is the constriction resistance, which increases during stripping as a consequence of void formation at the Li anode interface and the associated Li|LLZO contact area reduction and current focusing through the remaining Li|LLZO contact areas. The stripping tests were terminated when a cutoff voltage of 1.8V was reached, and the accessible stripping capacity of the anode was determined by the total stripping capacity up to the cutoff voltage. After the cutoff voltage of 1.8V was reached, the pressure on the cell was maintained and impedance spectroscopy was changed from galvanostatic mode (GEIS) under anodic load to potentiostatic mode (PEIS) at open circuit conditions. PEIS was used after cell polarization to continuously monitor the recovery of voids at the Li|LLZO interface [28].

This article is protected by copyright. All rights reserved.

Author Manuscript

Stripping in situ formed Li as a function of pressure at room temperature

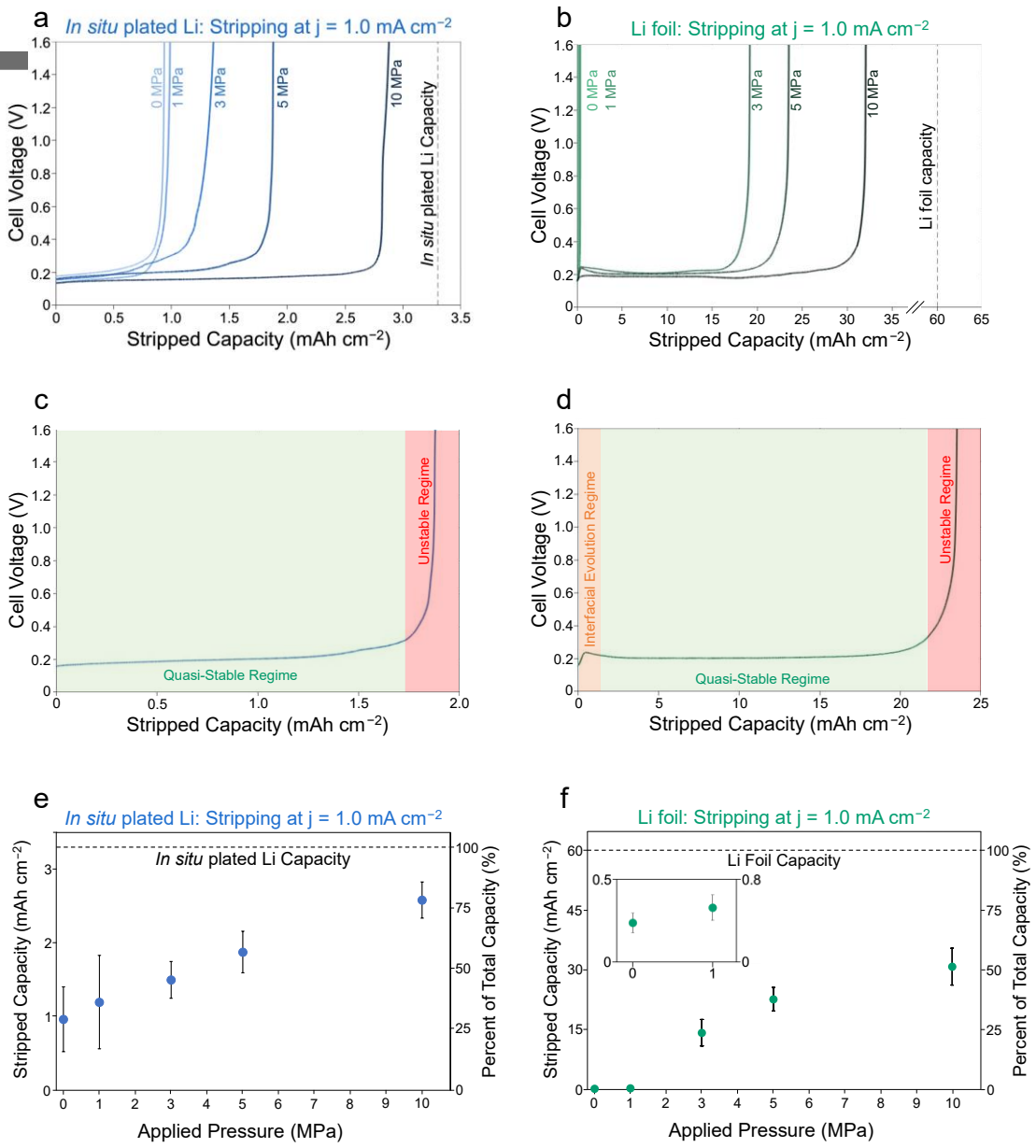


Figure 2. Voltage profiles for room-temperature (25°C) stripping under various pressures at a current density of 1 mA cm^{-2} for **a** *in situ* plated Li and **b** Li foil. Panel **c** shows the stripping voltage profile of an *in situ* plated Li anode at 5 MPa with quasi-stable (green) and unstable (red) shading. Part **d** shows the stripping voltage profile of a Li foil at 5 MPa, which includes an additional interfacial evolution regime (orange). The average accessible capacity as a function of pressure of n = 5 cells with standard deviation is shown in **e** for *in situ* plated Li and **f** for Li foil.

The voltage profiles for *in situ* plated Li during room-temperature (25°C) stripping at 1 mA cm^{-2} as a function of pressure are shown in Figure 2a. The dashed black line represents the total capacity available of *in situ* plated Li. Since 5 measurements were taken at each pressure for each cell type, a representative

This article is protected by copyright. All rights reserved.

Author Manuscript

voltage profile for a cell with the median accessible stripping capacity at each pressure is plotted to show trends in discharge behavior with pressure.

Figure 2a exhibits a similar shape of the voltage profile during stripping of *in situ* plated Li at all pressures at 1 mA cm^{-2}. Initially, the voltage rise is relatively flat with time until there is a sharp rise in the polarization of the cell. A previous investigation of Li|LLZO stripping using a three-electrode cell showed that this voltage increase can be attributed entirely to void formation at the working (stripping) electrode, and any roughening of the Li|LLZO interface at the counter (plating) electrode does not contribute significantly to the observed increase in interfacial resistance [8].

For stripping of *in situ* plated Li, the voltage profile is divided into two regimes as observed previously by Lee *et al.*: "quasi-stable" stripping, where the voltage profile is relatively flat, and "unstable" stripping, where the cell polarization rapidly increases (Figure 2c) [28]. In the quasi-stable regime, contact loss occurring at the Li|LLZO interface does not yet strongly increase the resistance, and therefore the voltage, of the cell. Previously, it was believed that Li depletion induced by the applied stripping current was balanced by Li replenishment through creep and vacancy diffusion in the quasi-stable regime. However, recent modeling results show that contact loss at the Li|LLZO interface does not directly correlate to a significant increase in cell resistance, and this effect may not become critical until >50% of the Li|LLZO contact is lost [46]. The unstable regime is characterized by a sharp increase in voltage until the cutoff voltage is reached, and stripping is terminated. In this regime, the lack of Li replenishment to the Li|LLZO interface becomes critical, leading to the abrupt increase in cell voltage. A previous study of Li stripping demonstrated that the unstable regime may be reached by two pathways: first, by local depletion of Li at the Li|LLZO interface due to void formation, or secondly, by global depletion of Li where the bare CC starts to contact the LLZO surface [28]. Stripping *in situ* plated Li at the high current density of 1 mA cm^{-2}, as shown in Figure 2a, leads to accessible capacities in the range of ~30-80% that of the total capacity of the *in situ* plated Li, meaning that ~20-70% of the plated Li remains at the working electrode after the unstable stripping regime is reached. Furthermore, the Nyquist plots before and after Li stripping show almost identical non-blocking behavior in the low-frequency region, even when ~80% of the plated Li inventory is stripped (Figure S3). Therefore, for

This article is protected by copyright. All rights reserved.

stripping of *in situ* plated Li at the conditions studied here (1 mA cm^{-2}, 25°C, 0-10 MPa) the abrupt increase in cell polarization in the unstable regime is attributed to void formation at the Li|LLZO instead of global depletion of Li at the working electrode.

The voltage profiles in Figure 2a show an increase in the applied stack pressure results in a delay of the transition between quasi-stable and unstable stripping for *in situ* plated Li cells. This observation is consistent with the hypothesis that Li|LLZO contact is evolving during the quasi-stable regime, leading to extended quasi-stable stripping at higher stack pressures. Higher stack pressures have been previously demonstrated to increase the creep deformation of Li, therefore delaying the transition from the quasi-stable to unstable regime [8]. The slope of the voltage profile in the quasi-stable regime also decreases with increased pressure, indicating that a higher stack pressure enhances the creep rate of Li towards the Li|LLZO interface during stripping. The accessible stripping capacity as a function of pressure is plotted in Figure 2e, where each point is the average of n = 5 cells, with the standard deviation represented by the error bars. The average stripping capacity increases with applied stack pressure, but the standard deviation in stripping capacity is higher at low pressures (0-1 MPa) compared to higher pressures (3-10 MPa). At 1 MPa, one cell demonstrated higher accessible stripping capacity than any of the cells at 3 MPa, but the average stripping capacity was higher at 3 MPa than at 1 MPa (Table S3). Although the yield strength of Li has been measured to be ~0.7 MPa in tension, the deformation of Li in compression at 1 MPa was previously shown to be limited when the Li metal is adhered to the LLZO surface and CC, as a result of frictional/adhesive forces [47,48]. Therefore, the accessible stripping capacity of *in situ* plated Li at the low stack pressures of 0 and 1 MPa is likely controlled by the initial Li|LLZO contact area and the Li diffusivity, as opposed to Li creep.

Since identical *in situ* Li plating and testing conditions are used for each cell, future work should focus on understanding the origins of the observed variability in the stripping performance of *in situ* plated Li, especially at low pressures (0-1 MPa). Stack pressures ≤ 1 MPa are desirable for commercial SSBs to maximize the pack-level energy density by limiting necessary controls on stack pressure in the pack, making the 0-1 MPa operating pressure range of commercial interest [7,24]. The highest accessible capacities that were measured at 0 and 1 MPa (1.5 and 2.0 mAh cm^{-2}, respectively) show that it is

This article is protected by copyright. All rights reserved.

Author Manuscript

Author Manuscript

possible to strip *in situ* plated Li in this system with 45-60% Coulomb efficiency at low stack pressures and high current densities.

Stripping Li foil as a function of pressure at room temperature

Figure 2b shows the voltage profiles for room-temperature stripping of Li foil electrodes under varying stack pressures. At pressures of 0 and 1 MPa, for Li foil, two stripping regimes are observed with similar characteristics to the quasi-stable and unstable regimes that were observed during the stripping of *in situ* plated Li. At these low pressures, the voltage rises quickly, and the resulting accessible capacity is small (<0.5 mAh cm^{-2}). Less than 1% of the total theoretical capacity of the Li foil anode can be stripped at these low pressures, as opposed to ~30% of the *in situ* plated Li capacity at the same pressures. Significant increases in accessible capacity are observed when the stack pressure is increased to 3 MPa (14 mAh cm^{-2}), and further improvements in accessible capacity are observed with increasing pressure up to 5 and 10 MPa (23 and 31 mAh cm^{-2}, respectively). This supports the hypothesis that at 0 and 1 MPa, Li diffusion and Li|LLZO contact area controls the accessible stripping capacity, while at 3-10 MPa, creep is the dominant factor.

When Li foil is stripped at 3-10 MPa, a new regime of stripping emerges prior to quasi-stable stripping, which we refer to here as the interfacial evolution regime (Figure 2d). In this regime, the voltage profile increases over the first ~0.5 mAh cm^{-2} until a peak is reached at ~0.18-0.25 V, after which the voltage plateaus (10 MPa) or slightly decreases before eventually plateauing (3 MPa and 5 MPa) (Figure S4). As shown in Figure S4, the interfacial evolution regime is still observed at 10 MPa, although the magnitude of the voltage increase is lower at 10 MPa than at 3 or 5 MPa. After reaching the quasi-stable stripping regime, the voltage remains relatively constant until the abrupt increase indicating the onset of the unstable stripping regime. The transition between the quasi-stable and unstable stripping regimes is delayed by increasing the applied stack pressure, similar to observations of stripping *in situ* plated Li. While higher stack pressures delay the transition to the unstable stripping regime, still only ~52% of the Li foil can be stripped at 10 MPa, leaving ~145 μm of Li foil inaccessible. The inevitable transition to the unstable regime of stripping despite the remaining Li inventory may be attributed to changing Li

This article is protected by copyright. All rights reserved.

Author Manuscript

mechanical properties as voids are healed under stack pressure or accumulation of impurities at the Li|LLZO interface during stripping. As the Li foil deforms plastically under stack pressure during stripping to mitigate void growth, the mechanical properties of Li may change as dislocations pile up at the Li|LLZO interface [9]. Further, creep deformation may be reduced as the Li thickness decreases from 300 μm at the start of stripping to ~155 μm when the unstable regime is reached [48]. Finally, Li foil is known to contain impurities which will not be transported through the LLZO, implying that these impurities will accumulate at the Li|LLZO interface during stripping, which could degrade stripping performance [49,50].

A similar initial voltage polarization behavior was observed in a previous study of stripping Li foil on LLZO. In that study, thicker Li foils were used (750 μm vs. 300 μm here), as well as a lower current density (0.5 vs. 1 mA cm^{-2} here) and stack pressure of 1.5 MPa [51]. The cell also exhibited polarization over the first ~0.5 mAh cm^{-2} of stripping to a higher voltage of ~0.9 V before decreasing in voltage and entering the quasi-stable stripping regime for the remaining 5.5 mAh cm^{-2} of stripping. The rising cell voltage in the first ~0.5 mAh cm^{-2} of stripping indicates loss of contact area between the Li and LLZO. Despite the changing contact area, the applied force to the cell remains constant during stripping. Generally, the nominal stack pressure is calculated by dividing the applied force to the cell by the full (projected) Li electrode area, and the applied force remains constant throughout the testing even as the Li|LLZO contact area may change. Therefore, the local pressure at the remaining Li|LLZO contact areas will increase when contact area is reduced during stripping. We hypothesize that at the peak voltage before the quasi-stable stripping regime, a "critical void fraction" is reached where the Li|LLZO contact area is reduced to a sufficient degree to increase the local pressure at remaining Li|LLZO contact areas above the Li flow stress. This hypothesis is visually represented in a schematic diagram in Figure S5.

After the "critical void fraction" is reached and Li begins to flow, the cell polarization decreases as some Li|LLZO contact area is re-formed. A new quasi-equilibrium Li|LLZO interface morphology is reached, where the degree of Li|LLZO contact is determined by the applied stack pressure. The polarization of the cells in the quasi-stable regime decreases as stack pressure is increased from 3 to 5 to 10 MPa, implying that there is a larger Li|LLZO contact area at higher stack pressures. We

This article is protected by copyright. All rights reserved.

hypothesize that this cell polarization behavior emerges at specific combinations of current density, pressure, and Li thickness where the current density is high enough to initially reduce the Li|LLZO surface contact, but the combination of pressure and Li thickness allows for flow of the Li before the cutoff voltage is reached. Even at identical pressure and current density conditions, the voltage response of the cell may vary depending on the thickness of the Li foil utilized due to enhanced creep deformation of thick Li foils [48].

Comparison of in situ plated Li and Li foil stripping behavior at room temperature

While the Li foil cells at higher pressures experience an initial voltage polarization followed by a plateau, *in situ* plated Li cells only go through the quasi-stable and unstable stripping regimes. At all pressures for *in situ* plated Li, the voltage remains relatively stable over the first 0.5 mAh cm^{-2} stripped, indicating that initial stripping of *in situ* plated Li may be more homogeneous than Li foil, leading to less initial Li|LLZO contact loss. When the unstable regime of stripping occurs and voltage abruptly increases, the voltage continues to increase to the cutoff limit instead of reaching a plateau, as observed for Li foil at 3-10 MPa. This difference in voltage response during stripping may suggest differences in the creep behavior of *in situ* plated Li versus Li foil when Li|LLZO contact area is reduced as indicated by cell polarization. *In situ* plated Li may be less able to creep than Li foil due to the low thickness of *in situ* plated Li, as well as possible differences in Li microstructure and purity [48]. When the unstable stripping regime is entered, the *in situ* plated Li has a thickness of only 2-10 µm compared to hundreds of microns thickness of Li foil, which may impact the ability of Li to deform to maintain Li|LLZO interfacial contact.

The stripping behavior of *in situ* plated Li and Li foil at low pressure (0 and 1 MPa) are compared directly in Figure S6. Although the total capacity of the Li foil is 18 times that of the *in situ* plated Li, a higher average accessible capacity is observed for *in situ* plated Li (1.0 and 1.2 mAh cm^{-2} at 0 and 1 MPa, respectively) compared to Li foil (0.2 and 0.3 mAh cm^{-2} at 0 and 1 MPa, respectively). As previously discussed, the deformation of Li, when adhered to the LLZO and CC, is very limited under 1 MPa stack pressure [48]. Therefore, it is likely that the accessible stripping capacity of Li at 0 and 1

This article is protected by copyright. All rights reserved.

Author Manuscript

MPa is controlled by the initial Li|LLZO contact area and the Li diffusivity as opposed to Li creep. Generally, the quality of the initial Li|LLZO interfacial contact is assessed by the Li|LLZO interfacial resistance from EIS, and it has previously been shown that the interfacial resistance is directly correlated to the Li|LLZO adhesive strength [52]. Previous work has optimized the Li foil|LLZO interfacial preparation to achieve negligible Li|LLZO interfacial resistance, and the same procedures are used in this work [15]. The Nyquist plots prior to stripping for the cells in Figure S6 are displayed in Figure S7. It can be observed that there are no major differences in the low frequency Li|LLZO interfacial region of the Nyquist plot between the *in situ* plated Li and Li foil cells.

While EIS is a generally accepted method of verifying interfacial contact in Li|LLZO cells, recent modeling studies of impedance contributions in SSBs have shown that relatively large differences in electrical contact area (60 versus 100% contact) may only have minimal effect on the observed constriction resistance, which does not increase proportionally to the Li|LLZO contact loss [46]. While *in situ* plated Li is observed to be highly conformal to the LLZO surface (Figure S1), direct imaging of the Li foil|LLZO interface is prevented due to the nature of the buried interface covered by 300 μm of Li foil, impeding cross sectional sample preparation through focused ion beam milling. Here, we suggest that despite having similarly low initial Li|LLZO constriction impedance, the interfacial contact can still differ between cells with different preparation methods, and this topic should be the focus of further investigation.

Finally, as mentioned above, both the Li|LLZO contact area and Li diffusivity could affect the Li stripping performance in these cells. Li foil, which is extruded and calendared to its final thickness, is observed to have differences in its microstructure compared to *in situ* plated Li using EBSD analysis (Figure S8) [41]. Each grain of the *in situ* plated Li is observed to span the full thickness of the plated Li, with grain boundaries perpendicular to the LLZO surface. However, for Li foil, the grain boundaries are not always perpendicular to the surface, and the full thickness of the Li foil is comprised of two or three grains instead of just one for *in situ* plated Li. The orientation of grain boundaries to the LLZO surface is important, as perpendicular grain boundaries are predicted to be ideal for fast Li transport during stripping [53]. Furthermore, the grain size itself is expected to impact Li diffusivity, with smaller

This article is protected by copyright. All rights reserved.

Author Manuscript

Li grains providing a higher fraction of grain boundaries, which may act as fast diffusion pathways. The *in situ* plated Li is observed to have grains ranging in size from ~7 – 50 μm, while the Li foil grain size ranges from ~20 – 250 μm. Therefore, this microstructural analysis supports the hypothesis that improved stripping behavior of *in situ* plated Li at 0 and 1 MPa, compared to Li foil, is due to improved Li diffusivity of *in situ* plated Li. However, it must be considered that the cross-sectional EBSD maps only capture 7-8 grains in each sample due to the large grain size of Li metal. Therefore, statistical grain size analysis cannot be performed here, and only preliminary conclusions can be made about the relative grain sizes observed between the samples.

Differences in purity between Li foil and *in situ* plated Li are also expected to affect the Li diffusivity. Attempts were made to conduct both inductively coupled plasma mass spectroscopy and inductively coupled plasma (ICP) optical emission spectroscopy to directly compare the purity of the *in situ* plated Li and Li foil. However, these attempts were unsuccessful due to easily ionizable element interference caused by the large concentration of Li ions in the solutions analyzed by ICP. Owing to the lack of a suitable analysis technique to determine the purity of *in situ* plated Li, we adopt the common assumption that *in situ* plated Li should have a higher purity than Li foil [28,40]. *In situ* plated Li is effectively "filtered" through the LLZO, a single-ion conductor, preventing contaminants from the Li foil counter electrode passing through the LLZO during *in situ* Li plating. Therefore, we propose that the diffusivity of *in situ* plated Li may be higher than that of Li foil due to both higher purity and smaller grain size.

Author Manuscript

This article is protected by copyright. All rights reserved.

Author Manuscript

Impedance spectra evolution during stripping

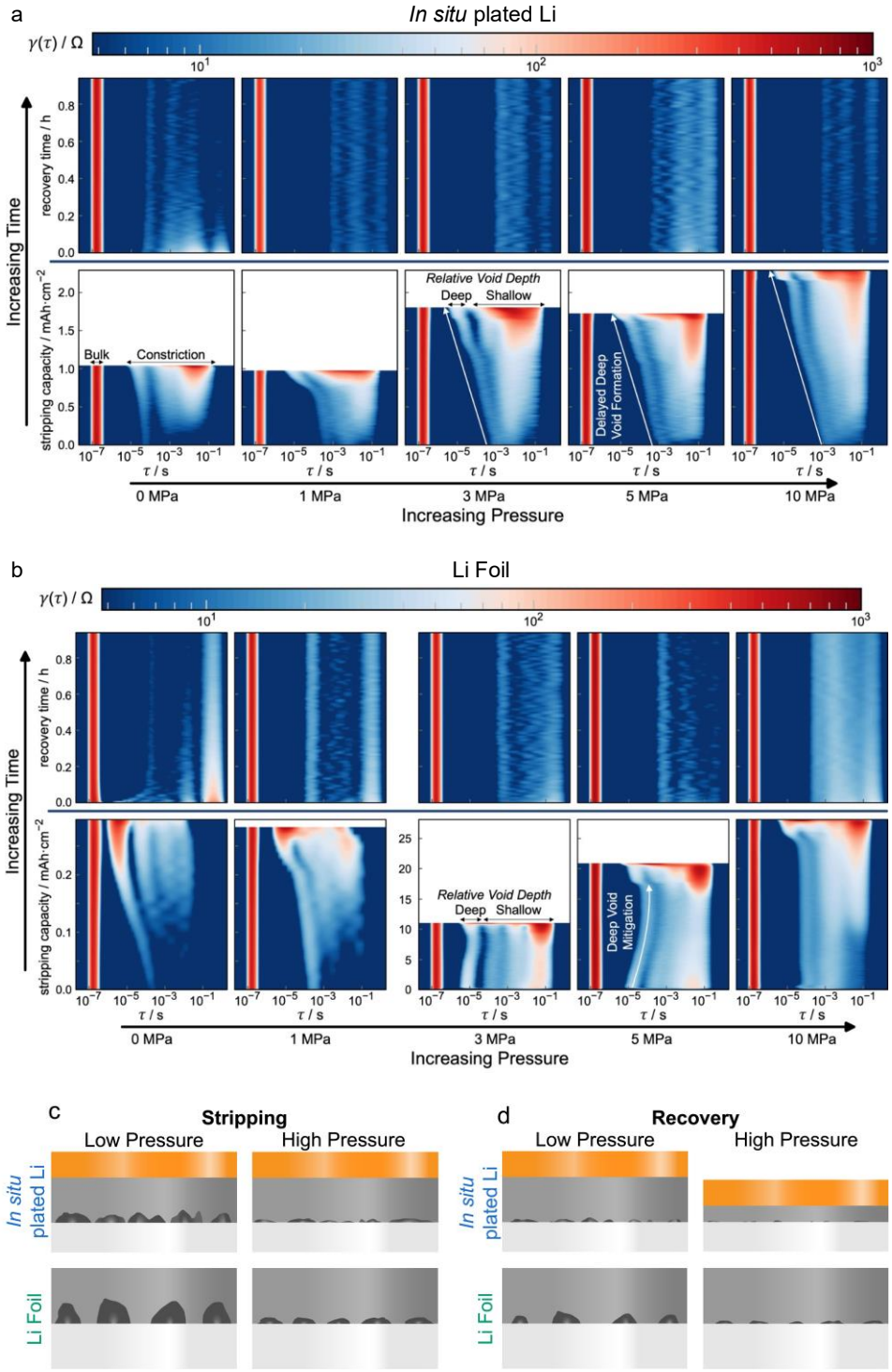


Figure 3. Impedance evolution, as represented by DRT contour maps, during both stripping and during recovery at open circuit conditions as a function of pressure for **a** *in situ* plated Li and **b** Li foil. Part **c** and **d** schematically depict the differences in interface morphology during stripping and recovery for the different Li types at low vs. high pressures.

This article is protected by copyright. All rights reserved.

Author Manuscript

To better understand the differences in stripping performance between *in situ* plated Li and Li foil, the GEIS stripping data was analyzed in more detail. The initial impedance spectra are plotted in a Nyquist representation, which shows a bulk contribution (Z_{Bulk}) at high frequencies and a small constriction contribution (Z_{Cstr}) at low frequencies (Figure S9). As the stripping capacity increases, the bulk signal remains unchanged, while the constriction signal starts to increase after a certain amount of capacity is stripped. The observed behavior is typical for Li void formation (i.e., contact loss), which in turn leads to the aforementioned phenomenon of current constriction. Recent theoretical results demonstrate that this geometric effect dominates the kinetics and polarization behavior at the LLZO interface rather than any charge transfer reaction [54].

As Li is stripped and the constriction impedance grows, differences in the shape of the low frequency semicircle (Z_{Cstr}) of the Nyquist plot can be observed at low versus high stack pressures for both Li foil and *in situ* plated Li (Figure S9). The semicircle corresponding to constriction impedance becomes depressed and less complete in the low frequency range as stack pressure is increased, meaning that the low frequency cutoff (1 Hz) is reached before the full constriction signal can be measured. Applying higher stack pressures changes the interface morphology and thus shifts the characteristic frequency of the constriction signal to lower frequencies, causing the loss of the complete constriction signal. This could be remedied by changing the frequency range of the GEIS to capture frequencies < 1 Hz. However, low frequency EIS data takes longer to collect than at high frequencies, so reducing the low frequency limit < 1 Hz greatly increases the time to acquire each impedance spectrum. In turn, this causes the impact of spectrum distortion from violating the steady state condition to become larger [25,26,55]. Therefore, it is generally not desirable to probe frequencies < 1 Hz for operando GEIS measurements during Li stripping.

The dependence of the characteristic frequency of the low frequency impedance semicircle (Z_{Cstr}) on the interfacial morphology underscores the geometric origin of current constriction. Eckhardt *et al.* demonstrated that the magnitude of the constriction resistance is not only determined by the contact area but also strongly depends on the 3D interfacial geometry in terms of spatial void distribution and void size [56]. Further, the constriction capacitance reflects the morphology of the voids (or pores) in the

This article is protected by copyright. All rights reserved.

Li metal. As a result, the time constant ($\tau = R \cdot C$) of the constriction signal depends on the void size and contact area determining the constriction resistance, and the contact area and the depth (d) of the voids influences the constriction capacitance ($C_{Cstr} \sim 1/d$). As a result, the time constant of Z_{Cstr} provides insights to the effect of Li type and applied stack pressure on the void morphology formed during stripping. Specifically, deeper voids will have smaller time constants, while shallower voids will have larger time constants because of the influence of void depth on the constriction capacitance. Qualitatively, this analysis can only differentiate between the deep or shallow voids that dominate the constriction impedance. Although voids are referred to here as a dichotomy between deep or shallow, a distribution of void depths is expected, leading to the observed wide band of relaxation times observed for the constriction effect. However, it is not possible to quantitatively assess the void depth or diameter based on this analysis.

To systematically analyze the time behavior of the interface impedance during stripping, the individual spectra collected during stripping are transformed into the time domain by calculating the underlying distribution function $\gamma(\tau)$ using distribution of relaxation times (DRT) analysis. For visual interpretation, the single DRT series are represented in a contour map (Figure 3a-b) where the relaxation time is plotted on the *x*-axis, the stripping capacity is plotted on the *y*-axis, and the color-code represents the amplitude of the distribution function $\gamma(\tau)$ at the different relaxation times. This means that the *x*-axis provides information about the electrochemical processes in the cell, the *y*-axis shows how these processes evolve over time during stripping, and the color visually indicates the resistance at a specific relaxation time.

Figure 3a shows the DRT contour maps as a function of pressure for stripping of *in situ* plated Li. The bulk resistance of the LLZO pellet can be observed at $\tau \sim 10^{-6}$ s across all samples and does not change in intensity or relaxation time as more Li is stripped. Signals observed from $\tau = 10^{-5} - 10^{-1}$ s are assigned to geometric constriction of the Li|LLZO interface. The broad relaxation time range is a consequence of the variation in void depth. Generally, two groups of interfacial constriction signals can be differentiated. The first, at $\tau \sim 10^{-5} - 10^{-4}$ s, corresponds to the constriction associated with formation of

This article is protected by copyright. All rights reserved.

Author Manuscript

deep voids (i.e., small capacitance), while the signal at $\tau \sim 10^{-3} - 10^{-1}$ s corresponds to constriction associated with the formation of shallow or lateral voids (i.e., large capacitance).

A comparison of the DRT contour maps as a function of pressure for stripping of *in situ* plated Li supports the previous hypothesis that stripping behavior is controlled by different factors at low pressures (0-1 MPa) and high pressures (3-10 MPa). At low pressures, the signal at $\tau \sim 10^{-4}$ s, which likely corresponds to deep voids in Li, emerges almost immediately during stripping. Applying pressure values ≥ 1 MPa causes the signal at $\tau \sim 10^{-4}$ s to instead appear slowly and continuously over many cycles. This leads to a sloped line on the left side of the constriction region on the DRT contour plot at 3-10 MPa, starting at roughly $\tau \sim 10^{-3}$ s at the beginning of stripping and ending at $\tau \sim 10^{-5}$ s when the voltage cutoff is reached. This agrees with the hypothesis that stack pressure delays the formation of voids at the Li|LLZO interface, and specifically indicates that pressure delays the formation of deep voids as opposed to lateral voids. This is illustrated schematically in Figure 3c. Unfortunately, reliable analysis of the signal at $\tau \sim 10^{-2}$-10^{-1} s arising from shallow voids is not possible for pressure > 3 MPa since the interface impedance is not fully captured in the measured frequency range.

The corresponding DRT contour maps as a function of pressure for Li foil are shown in Figure 3b. At 0 and 1 MPa, a high-intensity signal around $\tau \sim 10^{-5}$ s appears quickly during stripping. This implies that the cell polarization is being driven not by the formation of lateral voids, but by deep voids. This is different than the behavior observed at 0 MPa and 1 MPa for *in situ* plated Li, where a signal corresponding to deep void formation appears during stripping, but the intensity is still dominated by shallow or lateral void formation. At 3-10 MPa stack pressures, a different evolution of the DRT contour maps is observed compared to that of *in situ* plated Li at the same pressures, but again the analysis, especially at large relaxation times, is slightly affected by the incompleteness of the low frequency semicircles in the measured frequency range. While high stack pressures delay the appearance of the signal corresponding to deep voids for *in situ* plated Li, which leads to the sloping line on the contour plot, the signal corresponding to deep voids ($\tau \sim 10^{-5}$ s) appears after ~0.25 mAh cm^{-2} was stripped for Li foil (Figure S10). At 3 MPa and 5 MPa for Li foil, this time constant also shifts during stripping from

This article is protected by copyright. All rights reserved.

Author Manuscript

an initial value of $\tau \sim 10^{-5}$ s to $\tau \sim 10^{-4}$ s during the middle of the stripping, and finally back up to $\tau \sim 10^{-5}$ near the voltage polarization limit. This indicates that deep voids initially form quickly during stripping in the interfacial evolution regime (Figure 2d), but the void depth is then mitigated by the flow of Li as a result of to the applied stack pressure. Figure S10 also shows the presence of the interfacial evolution regime at 10 MPa applied stack pressure, where the time constant associated with constriction impedance initially shifts to the left before recovering. The DRT analysis specifically indicates that the deep voids, as opposed to shallow voids, are driving the voltage evolution behavior observed in Li foil cells at 0 and 1 MPa. Higher stack pressures (3-10 MPa) mitigate the deep voids that initially form during stripping of Li foil, and then lateral voids dominate the interfacial response in late-stage stripping at high pressures. The associated interfacial morphology predicted by DRT analysis is shown in Figure 3c.

Impedance spectra evolution during recovery

After the voltage cutoff limit is reached during stripping, the applied stack pressure on the cell is maintained while PEIS is performed at open circuit conditions. Therefore, changes in the DRT signal intensity and relaxation time after stripping can be monitored as a function of time to assess interfacial recovery. The recovery behavior of *in situ* plated Li over time is shown in Figure 3a. For all pressures, the constriction signals that are observed from $\tau = 10^{-5} - 10^{-1}$ s shift to longer relaxation times when stripping is terminated. This indicates a change in void morphology, specifically a decreased void depth leading to larger constriction capacitance. Compared to the final DRT signal during stripping, the signal corresponding to deep voids around $\tau \sim 10^{-5}$ s is not present by the time that the first full potentiostatic impedance spectrum is collected, which is roughly 30 seconds after stripping ends. Furthermore, a signal at a larger time constant ($\tau \sim 10^{-1}$) corresponding to more shallow voids is initially observed during recovery at 0 MPa, which was not present during stripping. The constriction signal overall shifts to the right during recovery, indicating that the depth of all voids is reduced during recovery compared to during stripping. This may indicate that under anodic load, deeper voids can be sustained in the Li

This article is protected by copyright. All rights reserved.

Author Manuscript

Author Manuscript

electrode than under open circuit conditions. After roughly 5 minutes recovery at 0 MPa, the signal corresponding to shallow voids fades and the Nyquist plot before and after cycling are nearly identical (Figure S11). Applied stack pressure generally increases the recovery rate of the interface, but it should be noted that recovery of the interface is only monitored by EIS. Due to the detection limit of voids at the Li|LLZO interface by EIS, the initial interfacial morphology may be different even if the recovered Nyquist plot appears identical to the one before stripping.

Recovery of the Li foil interface (Figure 3b) shows a similar general trend to that of *in situ* plated Li in that pressure increases the recovery rate of the Li|LLZO interface, and the constriction signals shift to longer relaxation times after stripping ends. However, at 0 and 1 MPa, there is a strong shift of the signal at $\tau \sim 10^{-5}$ s during stripping (corresponding to deep voids) to longer relaxation times at $\tau \sim 10^{-1}$ s after stripping. This may indicate a change in void morphology from deep to lateral voids occurs after stripping is ended. At these pressures, the Li|LLZO interface does not fully recover within the measured time (~1 hour). This is different than *in situ* plated Li, which recovers quickly (within ~5 minutes) at 0 and 1 MPa. The difference in recovery behavior between *in situ* plated Li and Li foil at 0 MPa is also predicted to be due to differences in Li diffusivity, as discussed previously. The predicted interfacial recovery morphology based on the DRT analysis is shown in Figure 3d. To further understand the void evolution at the Li|LLZO interface during stripping, a coupled electrochemical-mechanical model was developed.

This article is protected by copyright. All rights reserved.

Author Manuscript

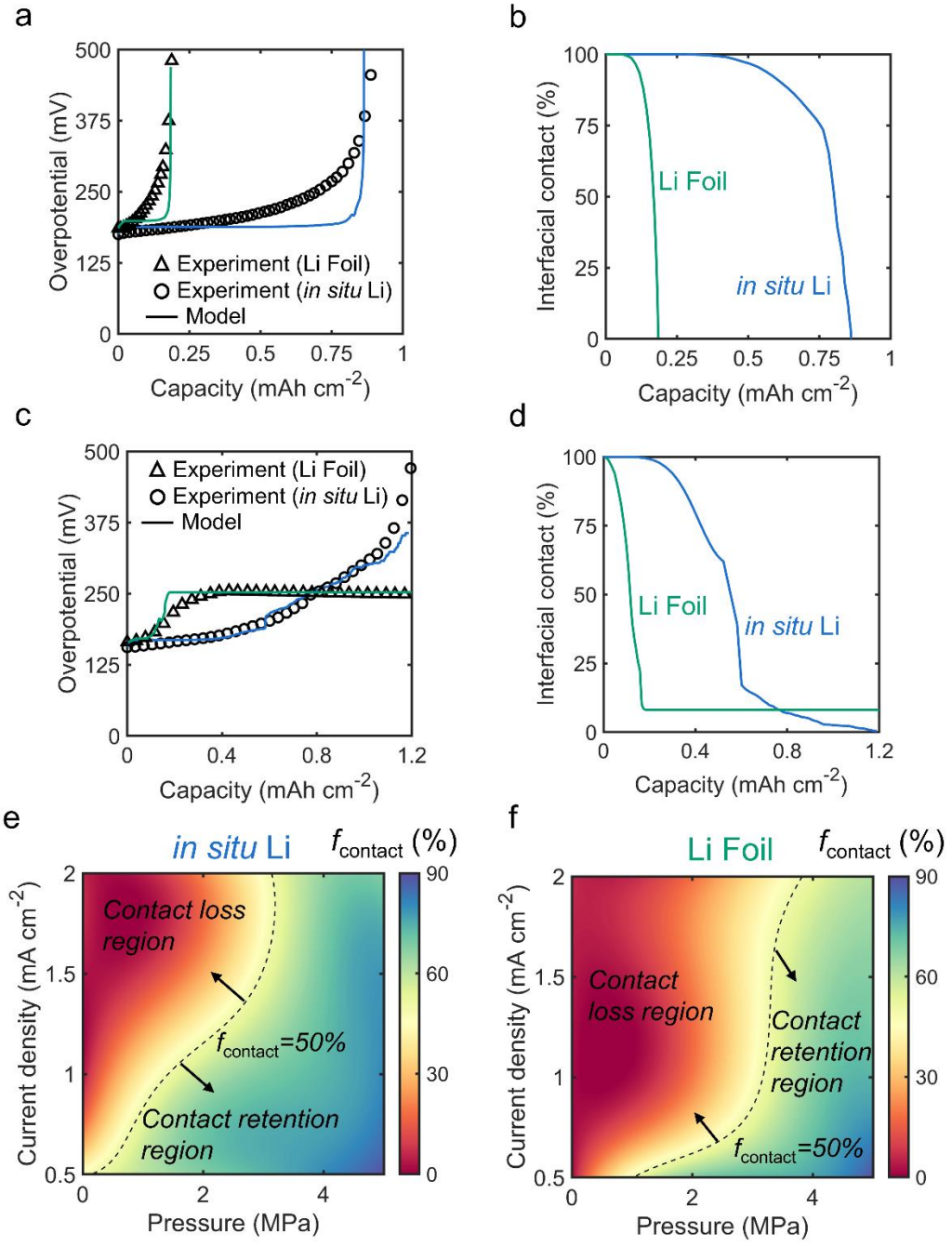


Figure 4. Impact of Li self-diffusion on the overall pressure-dependent stripping response of Li anodes in SSBs. Analysis of modeled overpotential (left panels) and interfacial contact evolution (right panels) signatures with galvanostatic stripping experiments at (**a-b**) 0 MPa and (**c-d**) 3 MPa stack pressure, with a current density of 1 mA cm^{-2}. Delineation of self-diffusion and pressure-dependent stripping response of (**e**) *in situ* plated Li and (**f**) Li foil anodes through demarcation of interfacial contact loss and retention regions under various operating conditions. The value of $f_{contact}$ represented in the phase maps indicate the percentage of retained contact area at a stripped capacity of 0.45 mAh cm^{-2}.

This article is protected by copyright. All rights reserved.

Author Manuscript

The electrochemical-mechanical processes at the Li|LLZO interface govern the differences in the stripping behavior at various operating conditions for Li (*in situ* plated and foil) anodes. To further understand the void growth dynamics at the Li|LLZO interface, we developed a coupled electrochemical-mechanical model that captures the heterogenous reaction kinetics, interfacial stresses and void depth distribution based on the applied pressure, current density and roughness profile of the SSE (~0.1 μm) [57]. The interfacial overpotential rise is predominantly dictated by the increase in geometric constriction impedance, which in turn is affected by the interplay of competing mechanisms that are driven by the electrochemical reaction at solid|solid point contacts, Li self-diffusion, contact mechanics, and viscoelastic creep. A description of the governing equations and methods associated with the modeling framework is provided in the Supplementary Information.

The voltage profile at 0 MPa offers key insights into the effect of self-diffusion associated with *in situ* plated Li and Li foil anodes. Li stripping at low pressure provides a heightened impact of Li self-diffusion due to the diminished influence of contact mechanics and creep deformation. The variations in critical stripped capacity (i.e., which is marked by a rapid increase of overpotential) is examined by evaluating the intrinsic self-diffusion of *in situ* plated Li (D_{Li} = 2 x 10^{-11} cm^2 s^{-1}) and Li foil (D_{Li} = 0.4 x 10^{-11} cm^2 s^{-1}) anodes. The magnitude of the Li self-diffusion directly relates to the rate of void healing, and subsequently the rise of the interface overpotential. Using the experimental electrochemical signatures at 0MPa, we employ our physics-based electrochemical-mechanical model to determine the intrinsic self-diffusion coefficients of these Li anodes, by mapping their concomitant rise of overpotential stemming from the rate of void healing at the Li|LLZO interface, primarily controlled by Li self-diffusion. A lower self-diffusion coefficient results in a lower critical stripping capacity, whereas higher self-diffusion facilitates lower interface overpotential through faster replenishment of Li to the Li|LLZO interface. Ideally, the Li self-diffusion coefficients determined through the model would be verified through experimental measurements. Previous studies have measured the diffusivity of thick Li foils using Sand's equation, as the assumption $t_0 << L^2 \cdot D_{eff}^{-1}$ is satisfied, where t_0 is the depletion time, L is the anode thickness, and D_{eff} is the effective diffusivity [26]. However, for thin *in situ* plated

This article is protected by copyright. All rights reserved.

lithium, this assumption is not met, and therefore, Sand's equation cannot be used to measure the diffusivity. Utilizing ^{6}Li pulsed field gradient nuclear magnetic resonance spectroscopy to measure Li diffusivity would require the challenging preparation of an *in situ* plated of ^{6}Li anode. Therefore, the important experimental work of directly measuring the diffusivity of *in situ* plated Li is recommended as future work to validate these models.

Figure 4a presents the modeling results compared to the experimental overpotential rise, signifying a higher stripped capacity of *in situ* plated Li due to higher self-diffusion. The model also reveals the corresponding contact evolution at the Li|LLZO interface (Figure 4b), where Li foil anodes suffer from a larger gradient in contact loss during low pressure stripping. Under identical operating conditions, the delayed loss of interfacial contact with stripped capacity and a slower overpotential rise of *in situ* plated Li is primarily facilitated by increased Li self-diffusion, moving Li more rapidly towards the Li|LLZO interface, thereby delaying void formation.

The contact at the Li|LLZO interface is considered to begin at 100%. Due to the sensitivity limits of EIS measurements, the exact percentage of initial interfacial contact cannot be quantitatively determined. Further, the impedance rise due to geometric constriction resistance is not directly inversely proportional to the contact area, so the exact interfacial contact area at the cutoff voltage cannot be determined. Therefore, the modeling of the changing Li|LLZO contact area should be interpreted as follows: 100% contact corresponds to the initial Li|LLZO interface, and 0% corresponds to the Li|LLZO contact area at the cutoff voltage, both of which are not possible to calculate from EIS measurements and would be difficult to measure from other techniques. Our model tackles this challenge by predicting the dynamic variation of interfacial contact area governed by the void growth evolution during stripping, that results in a heterogeneous electric potential field distribution at the Li|LLZO interface captured as the accrued overpotential. It is observed that the slower self-diffusion in Li foil anodes is marked by an 84% drop in contact retention with 0.06 mAh cm^{-2} of stripped capacity (Figure S12), whereas faster replenishment of voids through a higher diffusivity shows nearly a 6-fold increase in stripped capacity for *in situ* anodes for the same drop in interfacial area (Figure S12).

This article is protected by copyright. All rights reserved.

Author Manuscript

Author Manuscript

At moderate stack pressure conditions, the combined effect of contact mechanics, creep deformation and self-diffusion dictate the stripping behavior of Li anodes. Figures 4c and 4d present the overpotential and contact loss response of the representative anodes at 3MPa. A complete loss of interfacial contact is observed at 1.2 mAh cm^{-2} for *in situ* plated Li anodes. Although the slower self-diffusion in Li foil anodes indicates a faster overpotential rise with a steep gradient in contact loss within 0.4 mAh cm^{-2}, the higher creep deformation of thick Li foil anodes allows for a balance between slower self-diffusion and faster reaction kinetics, thus maintaining interfacial contact (~ 12% contact) during stripping. The Li self-diffusion response directly correlates to the rate of interfacial contact loss and voltage polarization. After 0.78 mAh cm^{-2} of stripped capacity (Figure 4d), despite the intrinsically faster Li self-diffusion we hypothesize that the reduced thickness of *in situ* plated anodes in contrast to the thick Li foil along with a lower creep rate cannot support the increasingly higher local currents at such low interfacial contact (~12%), thus progressing toward immediate cell failure. The prolonged sustenance of overpotential (~250 mV) and interfacial contact (~12%) of Li foil anodes (Figure 4d) indicates the pronounced creep deformation rate and contact mechanics aiding void suppression even at substantially higher local currents (~8.3 mA cm^{-2}) at the Li|LLZO interface. Further details on the incorporation of creep-driven void suppression and its mathematical framework are described in the Supporting Information. The rate of overpotential rise (i.e., differential voltage-capacity or dV/dQ) is much higher for the Li foil anodes (dV/dQ > 2 V cm^{-2} mAh^{-1}) during start of stripping, whereas *in situ* plated Li anodes with a higher self-diffusion coefficient exhibit lower peak signatures during stripping (Figure S15). Slower Li self-diffusion in the foil anodes results in a faster rate of contact loss, commensurate with the associated peaks in the dV/dQ signature. Thus, a combination of higher creep deformation and self-diffusion coefficient is essential to gain greater stripping efficiencies at low and moderate stack pressures.

Figures 4e and 4f demarcate regions of contact loss and retention at various operating conditions for *in situ* plated and foil anodes respectively. The impact of higher self-diffusion through a larger region of contact retention (Figure 4e) at low pressures is clear, while high stack pressures present negligible differences in interfacial contact between the two configurations. Figure 4f supports the hypothesis that

This article is protected by copyright. All rights reserved.

Author Manuscript

poor self-diffusion at low stack pressures can greatly affect the stripping performance, especially at higher current densities, while these effects are less pronounced during the start of stripping (Figure S14). Thus, Li-self diffusion presents as the predominant void healing mechanism at low stack pressures, while stripping at high stack pressures pose diminished contribution of void depth reduction from self-diffusion than creep.

Stripping behavior of in situ plated Li as a function of temperature

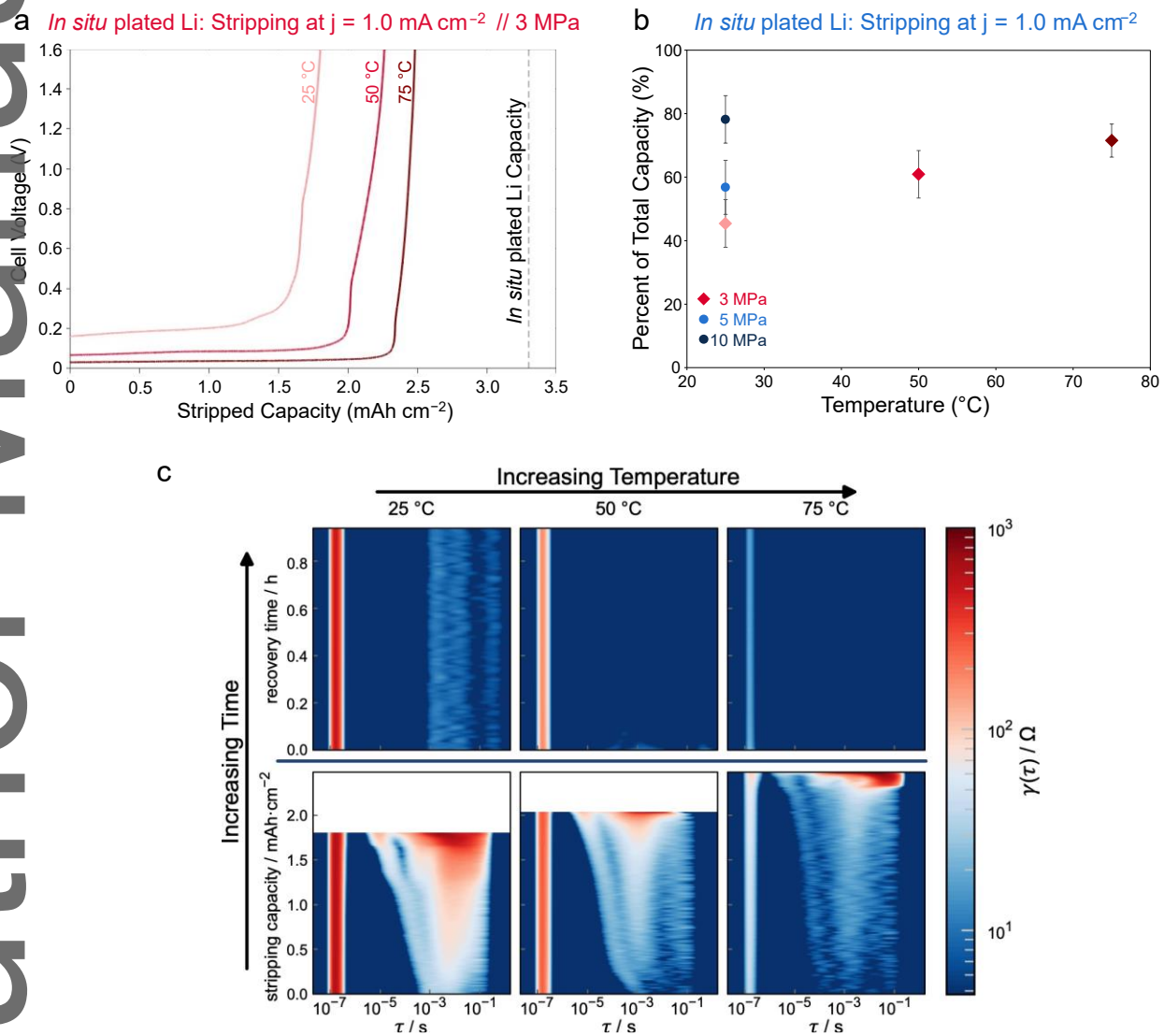


Figure 5. a Voltage profiles of *in situ* plated Li cells during stripping at 1 mA cm^{-2} and 3 MPa at 25, 50 and 75 °C. **b** The average stripping efficiency of n = 5 *in situ* plated Li cells as a function of temperature. **c** Impedance evolution, as represented by DRT contour maps, during stripping and recovery under open-circuit conditions as a function of temperature for *in situ* plated Li stripped at a pressure of 3 MPa.

This article is protected by copyright. All rights reserved.

Author Manuscript

In addition to the effect of pressure, the effect of temperature on the stripping capacity of *in situ* plated Li was also investigated. Due to the smaller standard deviation in stripping capacity at higher pressures, a constant stack pressure of 3 MPa was chosen, while temperature was varied to 25, 50 or 75°C during stripping. After the voltage cutoff was reached during stripping, the pressure and temperature were maintained and PEIS was conducted under open-circuit conditions to monitor the Li|LLZO interfacial recovery.

While an increased temperature is expected to increase the diffusivity and creep rate of Li, thereby enhancing the stripping performance, the effects of temperature on the measurement conditions must also be considered [47,58]. First, temperature is known to increase the ionic conductivity of LLZO, reducing the bulk resistance of the SSE and thus the overall cell voltage. Therefore, at higher temperatures the initial cell voltage is lower and a larger change in the voltage is required to hit the cutoff voltage. Additionally, the constriction impedance is proportional to the conductivity of the LLZO and will be lower at higher temperatures, even if the Li|LLZO contact area is identical between cells [56]. As a result, the degree of Li|LLZO contact loss must be larger to reach the cutoff voltage at elevated temperatures. In summary, the factors of Li diffusivity, Li creep, LLZO conductivity, and constriction impedance are all expected to contribute to increased accessible stripping capacities at elevated temperatures.

Figure 5a shows the voltage profiles of *in situ* plated Li stripped at 3 MPa as a function of temperature. Even though the initial slope of the voltage profile is significantly reduced at 50°C compared to 25°C, there is still an increase in the accessible capacity with temperature. This indicates that while the initial slope of the voltage profile can provide information on the stability of the Li|LLZO interface, it is not sufficient to predict the overall accessible capacity of the cell. Previous studies that analyzed the Li foil|LLZO interfacial stability as a function of temperature concluded that stripping was quasi-stable at a pressure of 1.25 MPa and stripping current of 0.2 mA cm^{-2} when the cell temperature was 50°C or higher[10]. However, only 3 mAh cm^{-2} out of a total Li foil capacity of 20 mAh cm^{-2} was stripped in the study, so full information on the effect of pressure and temperature on Li stripping behavior cannot be gained. Here, we show that even though the initial voltage profile slope is flattened by increased

This article is protected by copyright. All rights reserved.

Author Manuscript

temperature, differences in overall stripping behavior still exist when the Li foil electrode is stripped to depletion.

Figure 5b compares the average stripping efficiency as a function of temperature and pressure. Even though elevated temperatures significantly flatten the initial voltage profile, the average stripping efficiency is lower at 75°C / 3 MPa (72%) than at 25°C / 10 MPa (78%). This suggests that higher stack pressures may be more effective at encouraging Li creep during stripping than elevated temperatures, although the effect of temperature and stack pressure both combine to determine the overall deformation rate of Li metal.

The DRT contour maps as a function of temperature are shown in Figure 5c. As the conductivity of LLZO increases with temperature, the intensity of the bulk resistance signal at $\tau \sim 10^{-6}$ s decreases. Consequently, the overall resistance of the cell becomes lower as temperature is increased, and a lower degree of Li|LLZO contact is required to reach the voltage cutoff limit. At 75°C, the signal corresponding to deep void formation at $\tau \sim 10^{-5}$ s has a lower signal intensity than the signals at $\tau \sim 10^{-3} - 10^{-1}$ s compared to what is observed at 25°C or 50°C. Therefore, an increase in temperature may reduce deep void formation in the Li metal during stripping, and instead, more shallow or lateral voids are formed. This may be a result of the higher diffusivity or increased creep deformation of Li metal at higher temperatures. Finally, Figure 5c shows the recovery of the Li|LLZO interface monitored by PEIS after stripping. The recovery rate of the Li|LLZO interface increases with increasing temperature, again, due to enhanced Li diffusivity and deformability at higher temperatures.

The same coupled electrochemo-mechanical modeling framework as described above was also used to discern the effect of temperature on contact loss during stripping. Figures S13a and S13b illustrate the influence of temperature in maintaining conformal contact, which results in a minimal rise in overpotential and gradual loss of interfacial contact. With an increase in stripping temperature of *in situ* plated Li from 25°C to 50°C, a 35% reduction in contact at 1.2 mAh cm^{-2} is observed compared to 100% contact loss at 25°C. Higher temperatures improve the Li self-diffusion, Li creep rate, interfacial reaction kinetics and intrinsic ionic conductivity of the SSE manifesting as lower Ohmic loss at the start

This article is protected by copyright. All rights reserved.

Author Manuscript

of stripping (Table S2-S3). The degree of non-conformality is a direct consequence of the rate of mean void depth growth at various operating conditions (Figure S13c). An increase in stack pressure subdues the rate of rapid contact loss due to increased interfacial stresses and creep deformation, while higher temperatures elevate the strength of all void healing mechanisms resulting in greater contact retention during stripping.

Conclusions

In this study, we investigated the effects of pressure and temperature on the accessible stripping capacity of two types of Li metal anodes in SSBs. The discharge performance of thick (300 µm) Li foil anodes were compared to that of thin (16.5 µm) *in situ* plated Li metal anodes in "anode-free" cells. These findings reveal that at low pressures (0 and 1 MPa) and the high current density of 1 mA cm^{-2}, *in situ* plated Li anodes have higher accessible capacities than Li foil anodes despite having a much smaller total Li capacity.

For both Li types, a difference in stripping behavior is observed at low pressure (0-1 MPa) compared to higher pressures (3-10 MPa). At low pressures, the accessible stripping capacity is controlled by Li diffusion and the initial Li|LLZO contact area, while at high pressures, Li creep is the main factor influencing discharge performance. Furthermore, the collected GEIS data during stripping were analyzed through DRT to visualize the evolution of the Li|LLZO interfacial impedance over time. Due to the different constriction capacitance values that are associated with deep versus shallow void formation in the Li metal, signals in the DRT contour map can be associated with different Li void morphologies formed during stripping. Higher applied stack pressures were found to delay the formation of deep voids in *in situ* plated Li cells and mitigate formation of deep voids in Li foil cells. Additionally, it was observed that the formation of deep voids in Li foil at low pressure was more severe than that of *in situ* plated Li at low pressures. This difference in void morphology between the Li types at low pressure could indicate differences in initial the Li|LLZO contact area or Li diffusivity between Li foil and *in situ* plated Li. Furthermore, *in situ* plated Li recovered more quickly than Li foil, and

This article is protected by copyright. All rights reserved.

Author Manuscript

complete interfacial recovery was observed after only ~10 minutes even at 0 MPa applied stack pressure.

This work highlights the performance benefits of *in situ* plated Li compared to Li foils conventionally used in SSB research. Energy density targets require low amounts of excess Li in SSBs, and research must shift towards *in situ* plated Li to match commercially applicable systems. Further, this study suggests that stripping behavior of thick Li foils cannot be predicted to be unstable versus quasi-stable based on stripping a small amount of the total Li capacity present. Even if the initial voltage profile is flattened by applying temperature or pressure to delay void formation, the overall accessible capacity of the Li anode still differs overall. Finally, this study shows that DRT analysis of GEIS data can be used to discern differences in void formation during stripping of Li metal. This is a promising route to assess the impacts of pressure, temperature, and alloying interlayers on void formation in "anode-free" manufactured SSBs.

Acknowledgements

This work was supported by the Center for Mechano-Chemical Understanding of Solid Ion Conductors (MUSIC), an Energy Frontier Research Center funded by the U.S. Department of Energy, Office of Science, Office of Basic Energy Sciences under contract DE-SC0023438. Financial support by the BMBF Cluster of Competence FESTBATT (FB2-Char, 03XP0433D) and the BMBF project 03XP0509B (LiSi-2) is acknowledged by J.J., J. K. E. and T.F.

This article is protected by copyright. All rights reserved.

Author Manuscript

References

[1] Janek, J.; Zeier, W.G. A solid future for battery development. Nat Energy **2016**, *1*(9), 1–4.

[2] Hatzell, K.B.; Chen, X.C.; Cobb, C.L.; Dasgupta, N.P.; Dixit, M.B.; Marbella, L.E.; McDowell, M.T.; Mukherjee, P.P.; Verma, A.; Viswanathan, V.; Westover, A.S.; Zeier, W.G. Challenges in Lithium Metal Anodes for Solid-State Batteries. ACS Energy Lett **2020**, *5*(3), 922–934.

[3] Albertus, P.; Babinec, S.; Litzelman, S.; Newman, A. Status and challenges in enabling the lithium metal electrode for high-energy and low-cost rechargable batteries. Nat Energy **2018**, *3*, 16–21.

[4] Janek, J.; Zeier, W.G. Challenges in Speeding up Solid State Battery Development. Nat Energy **2023**, *8*.

[5] Megahed, S.; Scrosati, B. Lithium ion rechargeable batteries. J Power Sources **1994**, *51*, 79–104.

[6] Krauskopf, T.; Richter, F.H.; Zeier, W.G.; Janek, J. Physicochemical Concepts of the Lithium Metal Anode in Solid-State Batteries. Chem Rev **2020**, *120*(15), 7745–7794.

[7] Wang, M.J.; Kazyak, E.; Dasgupta, N.P.; Sakamoto, J. Transitioning solid-state batteries from lab to market: Linking electro-chemo-mechanics with practical considerations. Joule **2021**, *5*(6), 1371–1390.

[8] Wang, M.J.; Choudhury, R.; Sakamoto, J. Characterizing the Li-Solid-Electrolyte Interface Dynamics as a Function of Stack Pressure and Current Density. Joule **2019**, *3*(9), 2165–2178.

[9] Singh, D.K.; Fuchs, T.; Krempaszky, C.; Schweitzer, P.; Lerch, C.; Richter, F.H.; Janek, J. Origin of the lithium metal anode instability in solid-state batteries during discharge. Matter **2023**, *6*(5), 1463–1483.

[10] Klimpel, M.; Zhang, H.; Paggiaro, G.; Dubey, R.; Okur, F.; Jeurgens, L.P.H.; Kravchyk, K. V.; Kovalenko, M. V. Assessment of Critical Stack Pressure and Temperature in Li-Garnet Batteries. Adv Mater Interfaces **2024**, *11*(8), 1–8.

[11] Fuchs, T.; Haslam, C.G.; Moy, A.C.; Lerch, C.; Krauskopf, T.; Sakamoto, J.; Richter, F.H.; Janek, J. Increasing the Pressure-Free Stripping Capacity of the Lithium Metal Anode in Solid-State-Batteries by Carbon Nanotubes. Adv Energy Mater **2022**, *12*(26).

[12] Taylor, N.J.; Stangeland-Molo, S.; Haslam, C.G.; Sharafi, A.; Thompson, T.; Wang, M.; Garcia-Mendez, R.; Sakamoto, J. Demonstration of high current densities and extended cycling in the garnet Li7La3Zr2O12 solid electrolyte. J Power Sources **2018**, *396*, 314–318.

[13] Otto, S.K.; Moryson, Y.; Krauskopf, T.; Peppler, K.; Sann, J.; Janek, J.; Henss, A. In-Depth Characterization of Lithium-Metal Surfaces with XPS and ToF-SIMS: Toward Better Understanding of the Passivation Layer. Chemistry of Materials **2021**, *33*(3), 859–867.

[14] Otto, S.K.; Fuchs, T.; Moryson, Y.; Lerch, C.; Mogwitz, B.; Sann, J.; Janek, J.; Henss, A. Storage of Lithium Metal: The Role of the Native Passivation Layer for the Anode Interface Resistance in Solid State Batteries. ACS Appl Energy Mater **2021**, *4*(11), 12798–12807.

This article is protected by copyright. All rights reserved.

Author Manuscript

[15] Sharafi, A.; Kazyak, E.; Davis, A.L.; Yu, S.; Thompson, T.; Siegel, D.J.; Dasgupta, N.P.; Sakamoto, J. Surface Chemistry Mechanism of Ultra-Low Interfacial Resistance in the Solid-State Electrolyte Li7La3Zr2O12. Chemistry of Materials **2017**, *29*(18), 7961–7968.

[16] Sharafi, A.; Meyer, H.M.; Nanda, J.; Wolfenstine, J.; Sakamoto, J. Characterizing the Li-Li7La3Zr2O12 interface stability and kinetics as a function of temperature and current density. J Power Sources **2016**, *302*, 135–139.

[17] Lewis, J.A.; Sandoval, S.E.; Liu, Y.; Nelson, D.L.; Yoon, S.G.; Wang, R.; Zhao, Y.; Tian, M.; Shevchenko, P.; Martinez-Paneda, E.; McDowell, M.T. Accelerated Short Circuiting in Anode-Free Solid-State Batteries Driven by Local Lithium Depletion. Adv Energy Mater **2023**, *13*(12).

[18] Sandoval, S.E.; Lewis, J.A.; Vishnugopi, B.S.; Nelson, D.L.; Schneider, M.M.; Javier, F.; Cortes, Q.; Matthews, C.M.; Watt, J.; Tian, M.; Shevchenko, P.; Mukherjee, P.P.; McDowell, M.T. Structural and Electrochemical Evolution of Alloy Interfacial Layers in Anode-Free Solid-State Batteries. Joule **2023**, 1–20.

[19] Qian, J.; Adams, B.D.; Zheng, J.; Xu, W.; Henderson, W.A.; Wang, J.; Bowden, M.E.; Xu, S.; Hu, J.; Zhang, J.G. Anode-Free Rechargeable Lithium Metal Batteries. Adv Funct Mater **2016**, *26*(39), 7094–7102.

[20] Nanda, S.; Gupta, A.; Manthiram, A. Anode-Free Full Cells: A Pathway to High-Energy Density Lithium-Metal Batteries. Adv Energy Mater **2021**, *11*(2).

[21] Wang, M.J.; Carmona, E.; Gupta, A.; Albertus, P.; Sakamoto, J. Enabling "lithium-free" manufacturing of pure lithium metal solid-state batteries through in situ plating. Nat Commun **2020**, *11*(1), 1–9.

[22] Lee, Y.G.; Fujiki, S.; Jung, C.; Suzuki, N.; Yashiro, N.; Omoda, R.; Ko, D.S.; Shiratsuchi, T.; Sugimoto, T.; Ryu, S.; Ku, J.H.; Watanabe, T.; Park, Y.; Aihara, Y.; Im, D.; Han, I.T. High-energy long-cycling all-solid-state lithium metal batteries enabled by silver–carbon composite anodes. Nat Energy **2020**, *5*(4), 299–308.

[23] Haslam, C.; Sakamoto, J. Stable Lithium Plating in "Lithium Metal-Free" Solid-State Batteries Enabled by Seeded Lithium Nucleation. J Electrochem Soc **2023**, *170*.

[24] Kazyak, E.; García-Méndez, R. Recent progress and challenges for manufacturing and operating solid-state batteries for electric vehicles. MRS Bull **2024**.

[25] Krauskopf, T.; Hartmann, H.; Zeier, W.G.; Janek, J. Toward a Fundamental Understanding of the Lithium Metal Anode in Solid-State Batteries - An Electrochemo-Mechanical Study on the Garnet-Type Solid Electrolyte Li 6.25 Al 0.25 La 3 Zr 2 O 12. ACS Appl Mater Interfaces **2019**, *11*(15), 14463–14477.

[26] Krauskopf, T.; Mogwitz, B.; Rosenbach, C.; Zeier, W.G.; Janek, J. Diffusion Limitation of Lithium Metal and Li–Mg Alloy Anodes on LLZO Type Solid Electrolytes as a Function of Temperature and Pressure. Adv Energy Mater **2019**, *9*(44).

[27] Kasemchainan, J.; Zekoll, S.; Jolly, D.S.; Ning, Z.; Hartley, G.O.; Marrow, J.; Bruce, P.G. Critical stripping current leads to dendrite formation on plating in lithium anode solid electrolyte cells. Nat Mater **2019**, *18*(10), 1105–1111.

This article is protected by copyright. All rights reserved.

Author Manuscript

[28] Lee, K.; Kazyak, E.; Wang, M.J.; Dasgupta, N.P.; Sakamoto, J. Analyzing void formation and rewetting of thin in situ-formed Li anodes on LLZO. Joule **2022**, *6*(11), 2547–2565.

[29] Koshikawa, H.; Matsuda, S.; Kamiya, K.; Miyayama, M.; Kubo, Y.; Uosaki, K.; Hashimoto, K.; Nakanishi, S. Dynamic changes in charge-transfer resistance at Li metal/Li7La3Zr2O12 interfaces during electrochemical Li dissolution/deposition cycles. J Power Sources **2018**, *376*, 147–151.

[30] Ning, Z.; Jolly, D.S.; Li, G.; Meyere, R. De; Pu, S.D.; Chen, Y.; Kasemchainan, J.; Ihli, J.; Gong, C.; Liu, B.; Melvin, D.L.R.; Bonnin, A.; Magdysyuk, O.; Adamson, P.; Hartley, G.O.; Monroe, C.W.; Marrow, T.J.; Bruce, P.G. Visualizing plating-induced cracking in lithium-anode solid-electrolyte cells. Nat Mater **2021**, *20*(8), 1121–1129.

[31] Ning, Z.; Li, G.; Melvin, D.L.R.; Chen, Y.; Bu, J.; Spencer-Jolly, D.; Liu, J.; Hu, B.; Gao, X.; Perera, J.; Gong, C.; Pu, S.D.; Zhang, S.; Liu, B.; Hartley, G.O.; Bodey, A.J.; Todd, R.I.; Grant, P.S.; Armstrong, D.E.J.; Marrow, T.J.; Monroe, C.W.; Bruce, P.G. Dendrite initiation and propagation in lithium metal solid-state batteries. Nature **2023**, *618*, 287–293.

[32] Kazyak, E.; García-Méndez, R.; LePage, W.S.; Sharafi, A.; Davis, A.L.; Sanchez, A.J.; Chen, K.H.; Haslam, C.; Sakamoto, J.; Dasgupta, N.P. Li Penetration in Ceramic Solid Electrolytes: Operando Microscopy Analysis of Morphology, Propagation, and Reversibility. Matter **2020**, *2*(4), 1025–1048.

[33] Vishnugopi, B.S.; Dixit, M.B.; Hao, F.; Shyam, B.; Cook, J.B.; Hatzell, K.B.; Mukherjee, P.P. Mesoscale interrogation reveals mechanistic origins of lithium filaments along grain boundaries in inorganic solid electrolytes. Adv Energy Mater **2022**, *12*(3), 2102825.

[34] Chatterjee, D.; Naik, K.G.; Vishnugopi, B.S.; Mukherjee, P.P. Electrodeposition Stability Landscape for Solid–Solid Interfaces. Advanced Science **2024**, *11*(6).

[35] Wang, M.; Wolfenstine, J.B.; Sakamoto, J. Temperature dependent flux balance of the Li/Li7La3Zr2O12 interface. Electrochim Acta **2019**, *296*, 842–847.

[36] Zhang, X.; Wang, Q.J.; Harrison, K.L.; Roberts, S.A.; Harris, S.J. Pressure-Driven Interface Evolution in Solid-State Lithium Metal Batteries. Cell Rep Phys Sci **2020**, *1*(2), 100012.

[37] Zaman, W.; Zhao, L.; Martin, T.; Zhang, X.; Wang, Z.; Wang, Q.J.; Harris, S.; Hatzell, K.B. Temperature and Pressure Effects on Unrecoverable Voids in Li Metal Solid-State Batteries. ACS Appl Mater Interfaces **2023**, *15*(31), 37401–37409.

[38] Randau, S.; Weber, D.A.; Kötz, O.; Koerver, R.; Braun, P.; Weber, A.; Ivers-Tiffée, E.; Adermann, T.; Kulisch, J.; Zeier, W.G.; Richter, F.H.; Janek, J. Benchmarking the performance of all-solid-state lithium batteries. Nat Energy **2020**, *5*(3), 259–270.

[39] Vishnugopi, B.S.; Kazyak, E.; Lewis, J.A.; Nanda, J.; McDowell, M.T.; Dasgupta, N.P.; Mukherjee, P.P. Challenges and Opportunities for Fast Charging of Solid-State Lithium Metal Batteries. ACS Energy Lett **2021**, *6*(10), 3734–3749.

[40] Lee, K.; Sakamoto, J. Li Stripping Behavior of Anode-Free Solid-State Batteries Under Intermittent-Current Discharge Conditions. Adv Energy Mater **2024**, *14*(17).

This article is protected by copyright. All rights reserved.

Author Manuscript

[41] Fuchs, T.; Ortmann, T.; Becker, J.; Haslam, C.G.; Ziegler, M.; Singh, V.K.; Rohnke, M.; Mogwitz, B.; Peppler, K.; Nazar, L.F.; Sakamoto, J.; Janek, J. Imaging the microstructure of lithium and sodium metal in anode-free solid-state batteries using electron backscatter diffraction. Nat Mater **2024**.

[42] Boukamp, B.A. Electrochemical impedance spectroscopy in solid state ionics: Recent advances. Solid State Ion **2004**, *169*, 65–73.

[43] Wan, T.H.; Saccoccio, M.; Chen, C.; Ciucci, F. Influence of the Discretization Methods on the Distribution of Relaxation Times Deconvolution: Implementing Radial Basis Functions with DRTtools. Electrochim Acta **2015**, *184*, 483–499.

[44] Doux, J.M.; Nguyen, H.; Tan, D.H.S.; Banerjee, A.; Wang, X.; Wu, E.A.; Jo, C.; Yang, H.; Meng, Y.S. Stack Pressure Considerations for Room-Temperature All-Solid-State Lithium Metal Batteries. Adv Energy Mater **2020**, *10*(1), 1–6.

[45] Fuchs, T.; Haslam, C.G.; Richter, F.H.; Sakamoto, J.; Janek, J. Evaluating the Use of Critical Current Density Tests of Symmetric Lithium Transference Cells with Solid Electrolytes. Adv Energy Mater **2023**, *13*(45).

[46] Eckhardt, J.K.; Fuchs, T.; Burkhardt, S.; Klar, P.J.; Janek, J.; Heiliger, C. Guidelines for Impedance Analysis of Parent Metal Anodes in Solid-State Batteries and the Role of Current Constriction at Interface Voids, Heterogeneities, and SEI. Adv Mater Interfaces **2023**, *10*(8).

[47] LePage, W.S.; Chen, Y.; Kazyak, E.; Chen, K.-H.; Sanchez, A.J.; Poli, A.; Arruda, E.M.; Thouless, M.D.; Dasgupta, N.P. Lithium Mechanics: Roles of Strain Rate and Temperature and Implications for Lithium Metal Batteries. J Electrochem Soc **2019**, *166*(2), A89–A97.

[48] Haslam, C.G.; Wolfenstine, J.B.; Sakamoto, J. The effect of aspect ratio on the mechanical behavior of Li metal in solid-state cells. J Power Sources **2022**, *520*, 230831.

[49] Ho, A.S.; Westover, A.S.; Browning, K.; Maslyn, J.A.; Parkinson, D.Y.; Sahore, R.; Dudney, N.; Balsara, N.P. Comparing the Purity of Rolled versus Evaporated Lithium Metal Films Using X - ray Microtomography. **2022**, 10–14.

[50] Lang, J.; Jin, Y.; Liu, K.; Long, Y.; Zhang, H.; Qi, L.; Wu, H.; Cui, Y. High-purity electrolytic lithium obtained from low-purity sources using solid electrolyte. Nat Sustain **2020**, *3*(5), 386–390.

[51] Park, R.J.Y.; Fincher, C.D.; Badel, A.F.; Carter, W.C.; Chiang, Y.M. Ultrahigh Areal Capacity Li Electrodeposition at Metal-Solid Electrolyte Interfaces under Minimal Stack Pressures Enabled by Interfacial Na-K Liquids. ACS Appl Mater Interfaces **2023**, *15*(30), 36117–36123.

[52] Wang, M.; Sakamoto, J. Correlating the interface resistance and surface adhesion of the Li metal-solid electrolyte interface. J Power Sources **2018**, *377*, 7–11.

[53] Yoon, J.S.; Sulaimon, H.; Siegel, D.J. Exploiting grain boundary diffusion to minimize dendrite formation in lithium metal-solid state batteries. J Mater Chem A Mater **2023**, *11*(43), 23288–23299.

[54] Eckhardt, J.K.; Klar, P.J.; Janek, J.; Heiliger, C. Interplay of Dynamic Constriction and Interface Morphology between Reversible Metal Anode and Solid Electrolyte in Solid State Batteries. ACS Appl Mater Interfaces **2022**, *14*(31), 35545–35554.

This article is protected by copyright. All rights reserved.

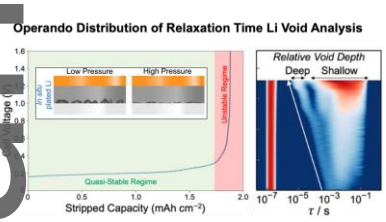
Author Manuscript

[55] Krauskopf, T.; Dippel, R.; Hartmann, H.; Peppler, K.; Mogwitz, B.; Richter, F.H.; Zeier, W.G.; Janek, J. Lithium-Metal Growth Kinetics on LLZO Garnet-Type Solid Electrolytes. Joule **2019**, *3*(8), 2030–2049.

[56] Eckhardt, J.K.; Fuchs, T.; Burkhardt, S.; Klar, P.J.; Janek, J.; Heiliger, C. 3D Impedance Modeling of Metal Anodes in Solid-State Batteries-Incompatibility of Pore Formation and Constriction Effect in Physical-Based 1D Circuit Models. ACS Appl Mater Interfaces **2022**, *14*(37), 42757–42769.

[57] Vishnugopi, B.S.; Naik, K.G.; Kawakami, H.; Ikeda, N.; Mizuno, Y.; Iwamura, R.; Kotaka, T.; Aotani, K.; Tabuchi, Y.; Mukherjee, P.P. Asymmetric Contact Loss Dynamics during Plating and Stripping in Solid-State Batteries. Adv Energy Mater **2023**, *13*(8).

[58] Kinzer, B.; Davis, A.L.; Krauskopf, T.; Hartmann, H.; LePage, W.S.; Kazyak, E.; Janek, J.; Dasgupta, N.P.; Sakamoto, J. Operando analysis of the molten Li|LLZO interface: Understanding how the physical properties of Li affect the critical current density. Matter **2021**, *4*(6), 1947–1961.



Operando DC - Distribution of Relaxation Time analysis studies the evolution of voids in Li anodes. The combination of techniques enables unprecedented insight into how pressure and Li thickness (*in situ* formed vs Li foil) affect void morphology during stripping.

This article is protected by copyright. All rights reserved.